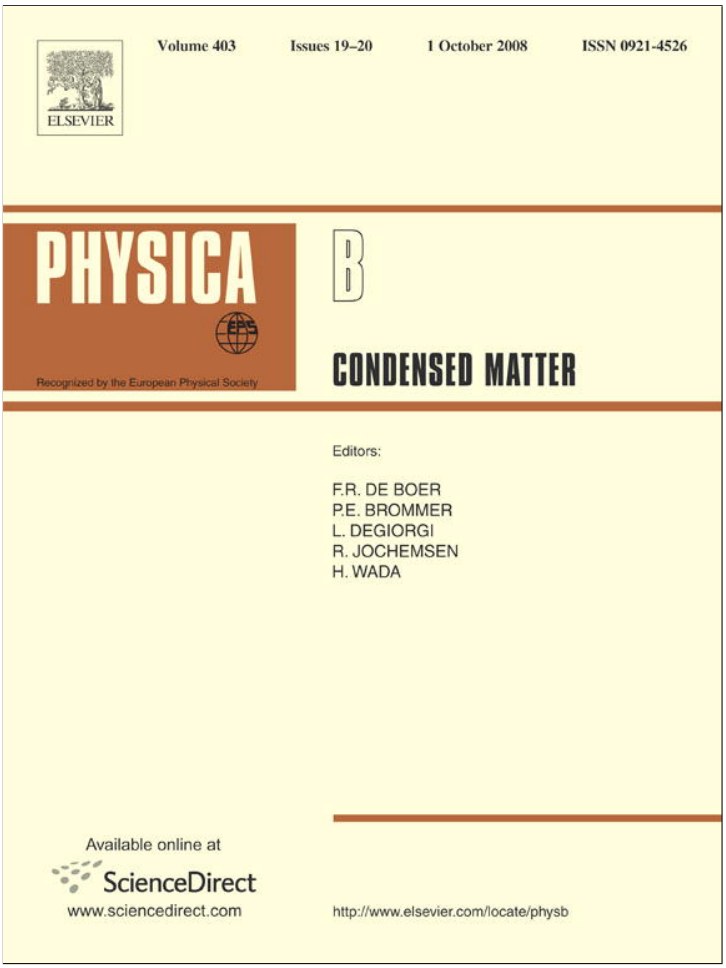

Physica B 403 (2008) 3774–3780

Contents lists available at ScienceDirect

Physica B

journal homepage: www.elsevier.com/locate/physb

Review

Nanometer-scale capacitance spectroscopy of semiconductor donor molecules

S.H. Tessmer [a,*], I. Kuljanishvili [b], C. Kayis [a], J.F. Harrison [c], C. Piermarocchi [a], T.A. Kaplan [a]

[a] Department of Physics and Astronomy, Michigan State University, East Lansing, MI 48824, USA
[b] Department of Physics and Astronomy, Northwestern University, Evanston, IL 60208, USA
[c] Department of Chemistry, Michigan State University, East Lansing, MI 48824, USA

ARTICLE INFO

Article history:
Received 18 June 2008
Accepted 7 July 2008

PACS:
71.22.+I
71.23.An
71.55.Eq
73.20.Hb
73.21.La
73.22.−f

Keywords:
Scanning probe microscopy
Dopants
Defects
Capacitance

ABSTRACT

We review recently reported scanned-probe capacitance measurements of electrons entering silicon donors in a gallium-arsenide heterostructure. Single-electron peaks were observed in the capacitance-versus-voltage curves. The precise voltage position of the peaks varied with the location of the probe, reflecting a random distribution of silicon within the donor plane. In addition, three broader capacitance peaks were observed independent of the probe location, indicating clusters of electrons entering the system at approximately the same voltages. These broad peaks are consistent with the addition energy spectrum of donor molecules, effectively formed by nearest-neighbor pairs of silicon donors.

Contents

1. Introduction

The ability to manipulate and probe small numbers of dopant atoms in semiconductors represents an emerging line of research, motivated by the continued miniaturization of semiconductor devices and potential applications where the dopants themselves form the functional part of a device [1–5]. Although donor properties are well understood with respect to bulk semiconductors, new questions arise in nanosystems such as the interaction between the donor confinement potential and the potential applied by nearby nanometer-scale electrodes. Moreover, because donors can be well approximated as hydrogenic atoms using an effective-mass theory, experiments on small numbers of donors have the potential to be a testing ground for fundamental predictions of atomic and molecular physics [6,7].

Electron tunneling spectroscopy through isolated dopants has been observed previously in two- and three-terminal devices such as gallium-arsenide double-barrier heterostructures and more

* Corresponding author. Tel.: +1 517 884 5660.
E-mail address: tessmer@pa.msu.edu (S.H. Tessmer).

0921-4526/$ - see front matter © 2008 Elsevier B.V. All rights reserved.
doi:10.1016/j.physb.2008.07.003

recently in gated silicon nanowires [8,9]. Moreover, Geim et al. [10] identified resonance in double-barrier devices, likely due to two closely spaced donors, effectively forming donor "molecules". In contrast to the experiment described here, these groundbreaking resonant-tunneling measurements were not able to resolve the characteristic electronic spectrum of the donor pairs. Here we review and discuss localized measurements of the electron addition spectrum of silicon donors in a gallium-arsenide heterostructure using a scanning probe technique—equivalent to a one-terminal device [11]. This study is the first example of single-electron capacitance spectroscopy (SECS) [12] performed directly with a scanning probe tip. In addition to the single-electron peaks, broader peaks were observed that are consistent with donor molecules, effectively formed by nearest-neighbor pairs of silicon donors [11].

2. Scanned-probe method

The technique is based on scanning charge accumulation imaging, which in this context can be considered as a scanned-probe version of SECS, pioneered by Ashoori and coworkers [12–14]. Fig. 1(a) shows schematically the main components of the experiment. The key sensing element is a metallic tip connected to a charge sensor constructed from cryogenic high-electron-mobility transistors, achieving a sensitivity of $0.01e$ $(\mathrm{Hz})^{-1/2}$ [15]. The measurement consisted of monitoring the tip's ac charging, as a function of dc bias voltage V_{tip}, in response to an ac excitation voltage V_{exc} applied to an underlying electrode. The measurement takes place with the sample and tip immersed in liquid helium-3 at a temperature of 280 mK.

The sample we employed was grown by molecular beam epitaxy and is of exceptional quality, similar to the samples used in previous SECS experiments that probed lithographically defined quantum dots [12,13]. The conduction band profile of the sample is shown in Fig. 1(b). A degenerately doped substrate acts as a metallic electrode. Above this is a two-dimensional (2D) electron layer. This represents an ideal base electrode from which charge can enter the higher layers in the sample. It is separated from the metallic substrate by a superlattice tunneling barrier; the tunneling rate into the 2D layer is an order of magnitude greater than the 20 kHz excitation frequency employed for all the measurements shown here. Hence for this experiment, the 2D layer can be regarded as being in ohmic contact with the substrate. Positioned 20 nm above the 2D conductor is the donor layer, which consists of silicon atoms confined to a single monolayer with respect to the z direction, but randomly positioned with respect to the x–y direction with an average density of $1.25\times10^{16}\,\mathrm{cm}^{-2}$. Charge may also become trapped in the cap layer, which is 30 nm above the donors.

For the local probe measurements, we used a PtIr tip with a radius of curvature of 50 nm and held its position fixed at a distance of 1 nm from the exposed GaAs surface. Under these conditions, the radius of the area over which we are probing is set mostly by the tip–donor-layer separation, which is approximately 60 nm [16]. Given the ~60 nm size of the probed area and average dopant density, we expect to be sensitive to about 140 donors. Fig. 1(c) shows an example of the expected energy landscape of the donor-layer quantum system, in the effective-mass picture [6].

In general, single electrons can be resolved by capacitance techniques at helium temperatures if the energy spacing to add successive electrons is on the millivolt scale or greater. As described in detail in Ref. [17], by measuring the capacitance C, we can detect charges entering the quantum system below the probe. Here for simplicity, we discuss the tip–sample system using a parallel-plate picture. A more accurate model that includes the fringing field of a sharp tip is discussed in detail in Ref. [16]. We define the addition energy ε_n as the energy for which the nth electron enters the donor layer. As V_{tip} increases from zero, relative to the 2D-layer chemical potential, the energy of the donor layer with respect to electrons decreases as $-\alpha_{\mathrm{tip}}eV_{\mathrm{tip}}$, where α_{tip} is the geometry-dependent proportionality constant. In other words, electrons in the underlying 2D electrode are pulled toward the donor layer. The first electron enters when $-\alpha_{\mathrm{tip}}eV_{\mathrm{tip}}$ crosses the ground state energy of the one-electron quantum state, $\varepsilon_1 = E(1)$. As V_{tip} increases further, the second electron will be induced to enter when $-\alpha_{\mathrm{tip}}eV_{\mathrm{tip}}$ equals the energy difference between two-electron and one-electron ground states, $\varepsilon_2 = E(2)-E(1)$. In general, $\varepsilon_n = E(n)-E(n-1)$, where we define $E(0)\equiv0$. The capacitance C is given by $C = \mathrm{d}q_{\mathrm{tip}}/\mathrm{d}V \propto \partial\langle n\rangle/\partial\mu$, where $\mathrm{d}V$ corresponds to the excitation voltage, μ is the donor-layer chemical potential, and $\langle n\rangle$ the expectation value for the number of electrons in the donor system [17]. Essentially, if an electron is able to enter the quantum system, the excitation voltage causes it to resonate between the system and the underlying electrode—giving rise to a peak in the capacitance.

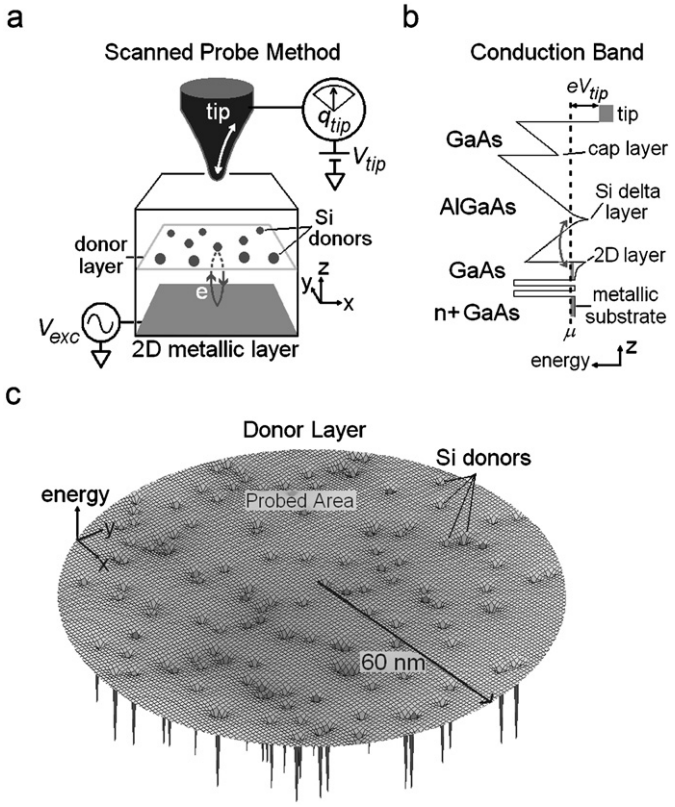

Fig. 1. (a) Schematic of the key layers in the gallium-arsenide heterostructure sample and the measurement technique. An excitation voltage applied to the 2D electrode can cause a charge to resonate between the Si donors and the 2D layer. This results in image-charge appearing on a sharp conducting tip. A cryogenic transistor attached directly to the tip is used to measure the charging. (b) Conduction band diagram of the sample. (c) Schematic of the area probed by the technique. The randomly positioned hydrogenic potentials represent ionized Si donors.

3. Measurements

Before introducing the local probe measurements, we first establish a baseline for the characteristic sample capacitance by showing a measurement we performed on a sample cut from the same wafer with a microfabricated gate electrode in place of the

tip. This is a more standard measurement, similar to the study performed by Hampton et al. [18]. Fig. 2(a) shows the resulting curve as a function of gate voltage, which we interpret in the following way: For sufficiently negative gate voltage, the 2D layer below the donors is depleted completely. As no charge can tunnel vertically, the signal is simply the substrate-to-gate capacitance. At around −1.0 V, as charge begins to enter the 2D layer; the capacitance increases, forming a step feature, as indicated. At around +0.1 V, charge begins to enter a second potential well formed below the cap layer. This gives a second capacitance step feature, as indicated.

For the voltage range displayed in Fig. 2(a), the signal showed negligible phase shifts and hence can be considered as purely capacitance. This also holds for the local probe data shown in Figs. 2(b–e). Also for both types of measurements, all voltages are plotted with respect to the effective zero voltage. This is the voltage for which no electric field terminates on the top electrode (gate or tip). It is shifted from the applied voltage by an amount equal to the contact potential, V_{contact}. For the PtIr tip used in the local probe measurements, $V_{\text{contact}} = 0.60$ V, as determined from *in situ* Kelvin Probe measurements [14]. For the gated-capacitance data, the observed shift in the curves implies $V_{\text{contact}} = 0.12$ V; this value agrees reasonably well with the reported work functions of Ti and Au, in comparison to Pt and Ir [19].

In addition to showing the accumulation of electrons in the 2D and cap layers, the gated-capacitance measurement allows us to estimate the density of ionized donors. This follows from the observation that the 2D electron system is fully formed at zero applied voltage. Of course, ionized donors introduce electric field; this in turn changes the slopes of the conduction band potential as shown in Fig. 1(b). These slopes must be sufficiently steep to allow the conduction band to dip below the Fermi level at the 2D location. Solving Poisson's equation with this constraint yields a density of ions equal to at least 90% of the growth Si density of $1.25 \times 10^{16}\,\text{cm}^{-2}$. Hence, most of the Si atoms have indeed donated an electron and are ionized at zero applied potential.

For the local probe measurements, we began each data run by scanning the tip in both tunneling and capacitance modes to check that the surface was sufficiently clean and free of major electronic defects [15]. To acquire the capacitance curves, we positioned the tip about 1 nm from the GaAs surface and held it at the fixed location while sweeping the tip voltage. To compensate for vibrations and drift effects, several curves were averaged together to achieve an acceptable signal-to-noise ratio. The resulting local capacitance curves consistently showed peaks in the vicinity of $V_{\text{tip}} \sim 0.5$ V, which were not present in the gated measurement.

To display the characteristic structure, Fig. 2(b) shows the average of three measurements (black dots) that exhibited the

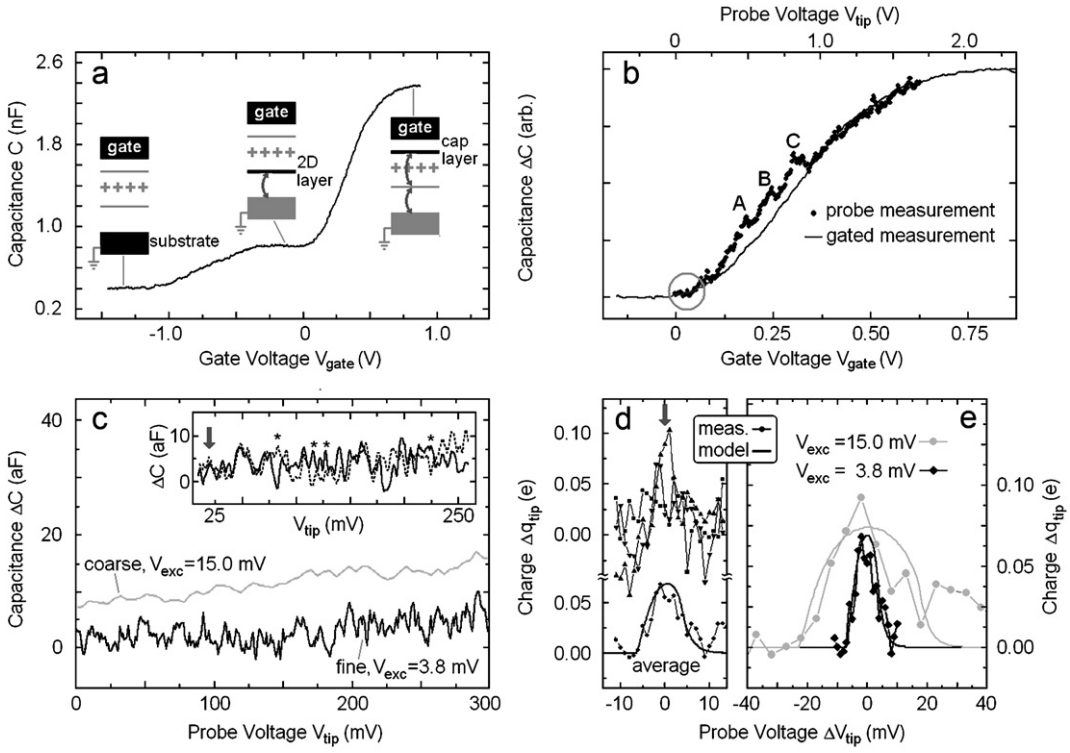

Fig. 2. (a) Gated-capacitance measurement performed using a planar gold–titanium gate deposited on the sample surface. The capacitance increases with gate voltage, forming three plateaus. The sketches show our interpretation as different layers below the gate accumulate charge. We do not display the data beyond 1.0 V, for which the signal begins to show a significant phase shift, indicating that charge is leaking directly onto the gate electrode. For this measurement, the gain of the capacitance signal was determined from sample geometry and gate area ($5.7 \times 10^{-7}\,\text{m}^2$). For all subsequent measurements, the signal was amplified with our HEMT charge sensor, for which the gain was measured independently. (b) Capacitance measured with our local probe superposed with the gated measurement. The local measurement is the average of measurements acquired at three locations. Three broad peaks labeled A–C were consistently observed. For both the local and gated curves, the voltage scales are plotted relative to the effective zero voltage, compensating for the contact potentials between the materials. The excitation voltage amplitude was $V_{\text{exc}} = 15$ mV rms for both curves. The vertical scale of the probe measurement is exaggerated greatly relative to the gated measurement. (c) Capacitance variation ΔC versus tip voltage curve over the voltage range shown in the gray circle in (b). These data were acquired at a single location but with two different excitation voltage amplitudes: "coarse", 15.0 mV rms and "fine", 3.8 mV rms. The inset shows two $V_{\text{exc}} = 3.8$ mV measurements acquired under identical conditions but with a time delay of 9 h. (d) Three curves acquired at the voltage marked by the arrow in (c) (same location) with an excitation voltage of 3.8 mV. The vertical scale has been converted to charge units and labeled as Δq_{tip} to indicate that we have subtracted away the background charge. Below we plot the average of the three curves. The measurement is compared to a model curve that shows the semi-elliptical peak shape expected for single-electron tunneling [13,16]. The width of the model curve is set by the 3.8 mV excitation amplitude; the asymmetry is caused by the lockin amplifier's output filter, which is included in the model. (e) Comparison of the peak shapes for isolated peaks for both the coarse and fine excitation amplitudes. The average data of (d) is re-plotted (black) along with an especially well-isolated peak observed at a different location and with the coarse excitation voltage of 15.0 mV (gray). The data are compared to two model curves that show the expected peak shapes for single-electron tunneling for the coarse and fine measurement parameters.

lowest noise, acquired at different locations. Three broad peaks, labeled A–C, are clearly resolved. For comparison, these data are superposed with the gated-capacitance curve (solid). Note that the two data sets have different voltage scales. This is expected given that the geometry-dependent alpha parameter should be different for the two measurements. For the gated measurement, the parallel-plate geometry and sample growth parameters give a proportionality constant of 1/4.0 with respect to the donor layer. For the local probe measurements, the relative scale factor between the two voltage ranges used in Fig. 2(b) implies $\alpha_{tip} = 1/10.8$. This is a reasonable value consistent with the expected tip–sample mutual capacitance [20,21]. Clearly, the broad peaks appear only in the local measurements; to help explain their physical origin, we first examine fine-structure peaks that also appear in the data.

Fig. 2(c) shows the capacitance variation versus tip voltage curve over the voltage range shown in the gray circle in Fig. 2(b). For these curves the background capacitance was subtracted away using a bridge circuit. Here we compare data acquired at a single location (not the average of three locations as in Fig. 2(b)) with two different excitation voltage amplitudes, as indicated. The coarse measurement (gray) is shifted vertically for clarity. The fine measurement (black) shows a series of small peaks. To gauge the reproducibility of the fine-structure peaks, the inset shows two measurements acquired under identical conditions but with a time delay of 9 h. We see the structure is reproducible partially, where the asterisks mark voltages for which peaks are missing or shifted in position. The observation that some peaks reproduce with almost identical shape and position highlights the level of stability the system achieves over several hours. The missing and shifted peaks likely reflect long time scale variations due to a small percentage of electrons trapped in deep metastable states such as Dx centers [22].

Fig. 2(d) shows three curves acquired at the voltage marked by the arrow in Fig. 2(c), with their average shown below. This peak was selected as it is relatively well isolated from neighboring peaks. For this plot we have converted the vertical scale to show the rms charge induced on the tip in units of the electron charge e. Fig. 2(e) shows isolated peaks for both the coarse (gray) and fine (black) excitation amplitudes. For the coarse data, the peak was especially well isolated. The data are compared to two model curves that show the expected semi-elliptical peak shapes for single-electron tunneling for the coarse and fine measurement parameters [16]. With regard to the widths of the peaks, in the low-temperature limit, the widths of the model curves are set by the excitation amplitudes; we see that the single-electron model agrees reasonably well with the measurements. With regard to the vertical scale, if all the electric field lines were captured by the tip, the magnitude of model single-electron peaks would be $0.99e$ and $0.92e$. However, to achieve a good fit, the heights of the model curves are scaled by 0.075. This peak height is roughly consistent with expected captured electric flux for single-electron charging within the donor layer, for which the scale factor should be approximately $\alpha_{tip} = 1/10.8 = 0.093$ [16,21]. Hence we conclude that the isolated fine-structure peaks likely reflect individual electrons entering the donor layer below the tip.

4. Analysis of broad peaks

Given that the fine-structure peaks likely mark electrons entering the donor layer, a natural explanation for the broader peaks (A–C) is that they are formed by clusters of several electrons entering at nearly the same energy. If we convert capacitance to charge units, we find that each peak corresponds to roughly 15 electrons entering the donor system, as described in more detail below. The reason such peaks were not seen in Fig. 2(a) and previous capacitance studies, such as Ref. [18], is probably the larger area probed in gated measurements. Micron-size areas are more likely to contain at least one severe defect or impurity that allows charge to penetrate the material and effectively short out interactions with the donor system [11].

What physics could give rise to the broad resonances observed in the local measurements? It is possible that dense groupings of the donors result in electron puddles acting as small quantum dots [23]. In that scenario, an ensemble of puddles that have nearly the same addition energy spectra could explain the peaks. However, given that the positions of donors should be random, it seems unlikely that 15 such puddles would form within a radius of only 60 nm with sufficiently similar characteristics. Considering the opposite limit, a candidate for identical quantum objects is single silicon donors. However, isolated Si donors in GaAs and AlGaAs can bind exactly two electrons [22], analogous to an isolated hydrogen ion in free space, which can also accommodate two electrons and form the negative H^- state. Hence, neglecting for the moment the interaction with the tip, an ensemble of isolated donors would yield only two broad peaks in the capacitance spectrum, whereas we observe three. Pairs of closely spaced silicon donors represent another candidate quantum system, which we will refer to as two-donor molecules (2DMs).

4.1. Configuration-interaction calculations

To explore the addition spectrum of 2DMs, we have calculated the electronic energies of two silicon donors separated by a distance d, but otherwise isolated. The calculations were performed using the configuration-interaction method [24,25] in the effective-mass theory [6,22]. In this approximation, a donor is regarded as a hydrogenic atom with an effective Bohr radius $a_0^* = 4\pi\varepsilon_0\kappa\hbar^2/m^*e^2$ and effective Rydberg energy $\mathrm{Ry}^* = e^2/8\pi\varepsilon_0\kappa a_0^*$, where ε_0 is the permittivity of free space, κ the dielectric constant, m^* the electron effective mass, and e the electron charge. In our system, Si donors reside in $Al_{0.3}Ga_{0.7}As$, for which $a_0^* = 7.3$ nm and $\mathrm{Ry}^* = 8.1$ meV [26]. The results for the first four electrons are plotted in Fig. 3(a). Interestingly, $E(3)$ is lower than $E(2)$ for large separations, but the two lines cross at $\sim 3a_0$. This means that at large separations, the molecule holds three electrons, similar to the H^- state; but for small separations only two electrons can be accommodated. The intuitive picture is that the neutral system can polarize and weakly bind the third electron. But this is prohibited for small separations for which the direct Coulomb repulsion dominates. This effect has been the subject of previous studies. We see that $E(4)$ is always higher energy than $E(3)$, hence the fourth electron is never bound.

To compare the calculations to our measurements, it is instructive to gauge the likelihood of finding 2DMs in our system. Fig. 3(b) shows the statistical nearest-neighbor distances for donors dispersed randomly within a 2D layer. Nearest-neighbor distances essentially follow Poissonian distributions [27]; selecting a donor at random, it can be shown that the probability to find its mth nearest neighbor between a distance R and R+dR is

$$\frac{(\pi R^2\rho)^{m-1}}{(m-1)!}2\pi R\rho\ \exp(-\pi R^2\rho)\mathrm{d}R,$$

where ρ is the 2D density. For the curves shown in Fig. 3(b), we used the nominal donor density of our sample, $\rho = 1.25\times10^{16}$ cm^{-2}. With regard to 2DMs, we see that on average the first nearest neighbor will be less than a_0^* away. Hence we expect that many 2DMs will be present in the experiment. However, as shown in Fig. 3(a), the configuration-interaction calculations predict only two bound electrons for these small separations;

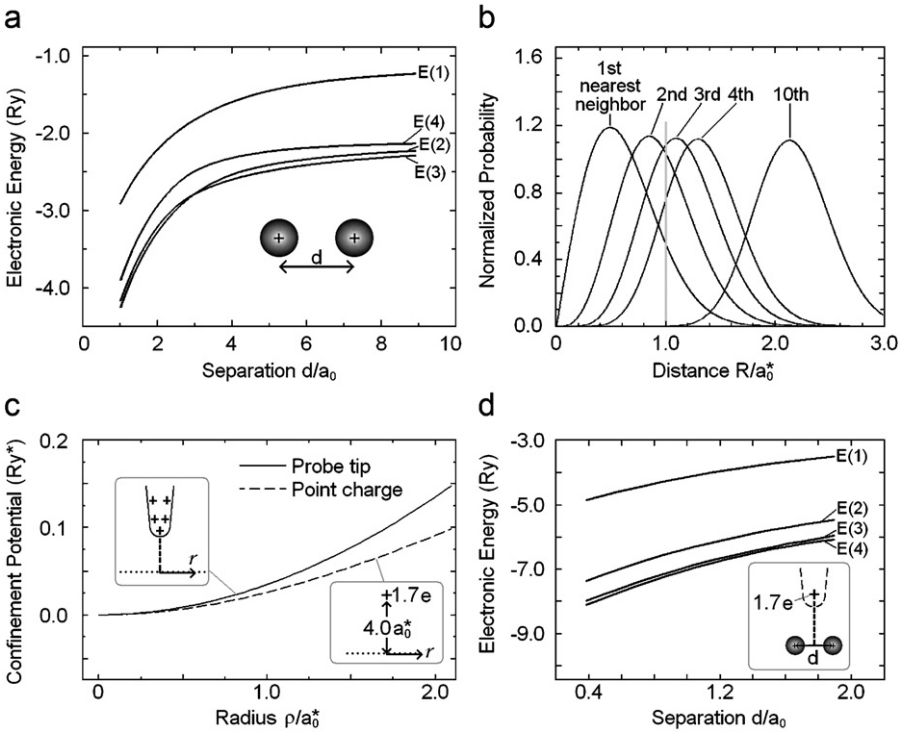

Fig. 3. (a) Configuration-interaction calculation of the electronic energies of two donors separated by a distance d, but otherwise isolated, as shown in the inset. At small separations, the model predicts two bound electrons for each donor molecule. (b) Statistical nearest-neighbor distances for donors in our system, calculated using the nominal growth density of donors in our sample. For comparison to theory, the distances are given with respect to the effective Bohr radius. (c) (Solid) calculated tip-confinement potential in the donor layer [11,16]. (Dashed) image-charge approximation incorporated into the configuration-interaction calculations. A point charge of $1.7e$ was employed at a distance of $4a_0$, as indicated in the inset. (d) Revised configuration-interaction calculations including the rough approximation for the tip potential. This revised model predicts four bound electrons for each donor molecule—even for separations less than a_0.

this is inconsistent with our observation of three peaks. With regard to isolated donors, Fig. 3(b) shows that only a small fraction of the donors will have no neighbors within one effective Bohr radius. Hence it is unlikely that isolated donors will contribute significantly to the addition spectrum.

Thus far we have neglected the perturbative influence of the tip. With respect to the donor-layer plane, the positive tip voltage gives a curved background potential that tends to increase the confinement. We can therefore improve our theoretical model by including an image-charge in the calculations that approximates this potential. The solid curve of Fig. 3(c) shows the expected confinement potential for $V_{\mathrm{tip}} = 0.45\,\mathrm{V}$, which is the potential in the vicinity of peak A; the dashed curve is the image-charge approximation incorporated into the configuration-interaction calculations. We see the image-charge approximation is somewhat weaker than the expected confinement; moreover we take this potential as fixed, even though the tip voltage varies during the measurement. Hence, this is a very rough approximation of the tip's influence, necessitated by the computationally intensive nature of the calculations. The decision to err on the side of weak confinement is justified by the fact that the confinement effect weakens for donors not directly below the tip. Fig. 3(d) shows the corresponding 2DM calculations for the electronic energies for the first four electrons. In this case we see that $E(3)$ is lower than $E(2)$ even for small separations. Hence this spectrum shows that the third electron will always be bound. Moreover, the fourth electron is also bound, but very weakly. All subsequent electrons are unbound in this calculation.

4.2. Influence of non-nearest neighbors

In addition to interactions with the tip and with nearest-neighbor donors, a complete model suitable to directly simulate the measurements must also include the effects of the non-nearest neighbors. We can gain insight into the physics of the system by comparing rigorous calculations of the binding energy of the first electron $E(1)$ to a very simple Coulomb-shift approach. The black curves of Fig. 4(a) compare the rigorous binding energy of the two-atom molecule (solid) to a curve derived by shifting the binding energy of an isolated H atom by the Coulomb energy of a charged neighbor at a distance d: $e/4\pi\varepsilon_0 d$ (dashed). We see that for distances greater than a_0, the two agree to within a precision of ~15%. The gray curves make a similar comparison for a three-atom equilateral triangle, reproduced from Ref. [10], and an isolated H atom Coulomb shifted by two neighbors at a distance d. We see that this simple-minded approach does a surprisingly good job of predicting the addition energy for the first electron. However, as the unshifted energies are based on an isolated H atom, it is too simplistic to generate the full addition spectra for two-atom molecules.

Motivated by these ideas, we have developed a model that extends the 2DM configuration-interaction calculations to account for non-nearest neighbors. Fig. 4(b) schematically introduces the method, which follows essentially a Monte Carlo approach [11,27]. We consider a 2D area of $\pi(60\,\mathrm{nm})^2$ with 140 donors, labeled i in the figure. We position the donors randomly within the area and group them into 70 nearest-neighbor pairs, labeled k. Each pair has assigned to it an addition spectrum $\varepsilon^k_{1,2,3,4}$ based on the separation of the two atoms as given by Fig. 3(d), indicated in gray in Fig. 4(b). To simulate the capacitance-versus-voltage curve, we consider the Coulomb shift U_i^k of every quantum level due to all the other donors. This leads to an ensemble of 2DM energy levels, resulting in broad peaks similar to the measurements. The width of the peaks is ~1 Ry*, arising mostly from the variation in Coulomb shifts as each 2DM has a different configuration of neighbors [11,16].

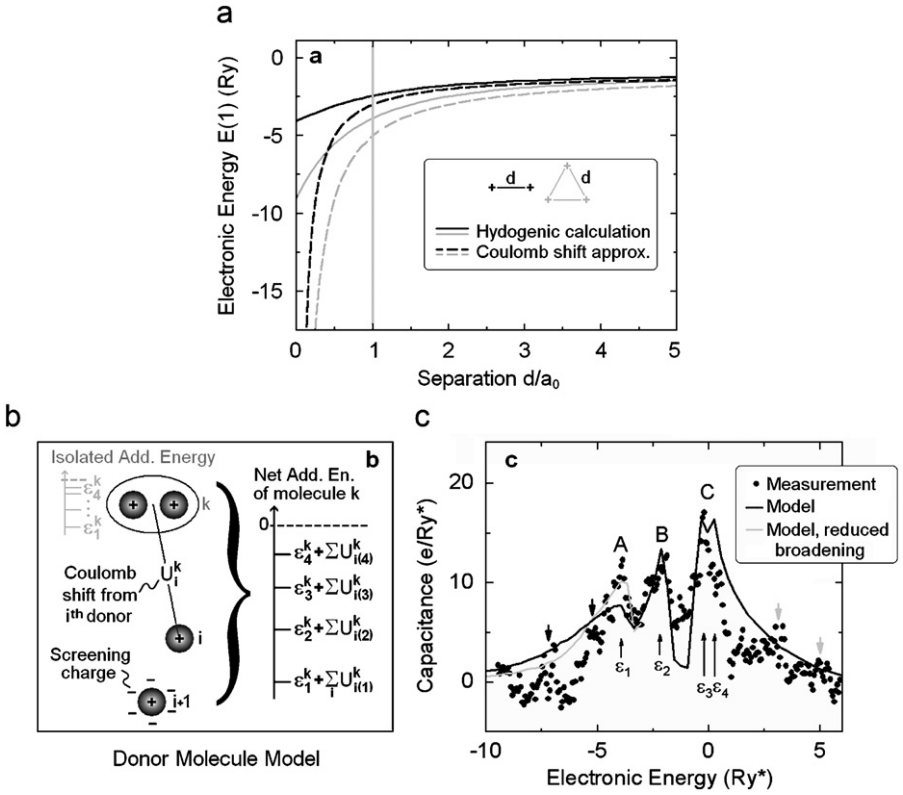

Fig. 4. (a) A comparison between a rigorous calculation of the binding energy of the first electron (solid) and a simple Coulomb-shift approximation (dashed). The black curves correspond to two donors and the gray curves correspond to three. The solid gray curve is reproduced from Ref. [10]. (b) Schematic representation of the modeling procedure. The net addition energy for any given molecule depends on the total Coulomb shift from all non-nearest neighbors. As indicated by the parentheses, we account for the fact that this shift will be different for successive electrons due to changes in the screening charge of surrounding donors—as electrons enter other pairs. (c) Comparison between the model and the measured data. The background capacitance (Fig. 2(b) solid curve) has been subtracted from the local measurement (Fig. 2(b) dots) to isolate the peaks. We display both the measured and modeled curves with the same horizontal scale of Ry* and vertical scale of electrons per Ry*. Although the match between experiment and theory is not exact, the overall agreement suggests that the donor-molecule model captures the correct physics. The gray curve addresses the discrepancy with regard to peak A, for which the predicted peak is significantly broader than the measurement; here we have reduced the broadening in the calculation by positioning the 2D layer 8 nm closer to the donor layer, which tends to sharpen the resonances [11].

To make the model realistic, we consider that the ionization of the system changes throughout the measurement. For example, for the first electron to enter the area, we assume all the donors are ionized. Hence we calculate the Coulomb shifts for each pair $k\sum_i U_i^k$ using a charge of $+e$ for all donors. In this case, the pair that has the lowest energy $\varepsilon_1^k + \sum_i U_i^k$ receives the electron, filling its first state and thus contributing to the capacitance at this energy. For all subsequent electron additions into other pairs, we must consider that this particular pair no longer has two fully ionized atoms. In other words, for the second electron, which would likely enter some other pair, the Coulomb shifts will be slightly reduced due to the previous charge that has already entered the system and partially neutralized one pair of atoms. To account for this effect in a straightforward way, we assume perfect screening: every time an electron enters a 2DM, we add $-e/2$ to each atom of the pair. The model also includes the screening effect of the nearby 2D layer in our sample by using appropriately positioned image charges. Our routine calculates capacitance curves in this way, using the effective Rydberg as the energy scale. To generate smooth data that represents the average capacitance curve, we perform the calculation for hundreds of random ensembles and average the results together.

4.3. Comparing the calculation and measurement

Fig. 4(c) shows a comparison between the observed capacitance peaks and the full 2DM model, where we have subtracted the background capacitance from the local measurement to better display the peaks. The data are displayed in units of effective Rydbergs and shifted horizontally so that peak C is at zero. This is consistent with peak C lying near zero effective Rydbergs, the energy above which the electrons are unbound. No other free parameters were employed in the comparison. We see that the model predicts that three broad peaks with distinct shapes will be observable as shown by the black curve. The reason the model gives only three peaks despite the fact that there are four electrons per molecule is simple: both $\varepsilon_3 = E(3) - E(2)$ and $\varepsilon_4 = E(4) - E(3)$ are less than 1Ry*, hence they are not resolvable as individual peaks. The reason the peaks have distinct shapes is more subtle, arising from the ionization effects described above. Essentially, for the second electron additions, on average there are fewer ionized charges in the donor layer than for the first-electron additions. Therefore the overall Coulomb shift is reduced for the second electrons, which form peak B, as well as the broadening effect due to the randomness of the donor positions. For this reason the model predicts that peak B will be sharper than peak A. The shape of peak C is also broadened by the proximity of ε_3 and ε_4. Comparing the model to the data, we see that the charge magnitude and relative energy spacing of the model peaks are in good agreement with the measurements, with peaks A and B corresponding to the average addition energies of the first and second electron peaks $\varepsilon_{1,2}$ as indicated; the model predicts that the third and fourth electron peaks $\varepsilon_{3,4}$ will be unresolved, consistent with peak C. Hence, we believe that the 2DM model captures the key physics of the system.

The model does not account for all of the features in the data, in particular the smaller peaks indicated by the downward-pointing arrows in Fig. 4(c). One reason for the discrepancy may be that the model does not account for clusters of three or more donors. Among these larger clusters, the contribution of three-donor molecules (3DMs) should be most prominent; as discussed in Ref. [11], on average 12 3DMs should be present in the probed area, compared to 26 2DMs (and only six four-donor molecules). Although we have not developed a simulation to account for 3DMs, we can use the results of the 2DM model as a rough guide for the behavior of the 3DM first-electron additions. For both 2DMs and 3DMs, the first-electron addition ε_1 can be estimated using the expression $\varepsilon_1 = -Z^2$, where Z is the nuclear charge of the ions and the units of energy are Ry*; this is exact in the limit of zero separation of the ions within the molecule, in which case we have a hydrogenic potential (and no electron–electron interactions to consider as this is the first electron). The expression gives $\varepsilon_1^{2DM} = -2^2 = -4\text{Ry}^*$, in surprisingly good agreement with the average first-electron peak calculated by the full 2DM model, as shown in Fig. 4(c). The agreement results from an approximate cancellation of three effects: on average the two molecules are separated by $1.2a_0^*$, which tends to increase ε_1; however, the Coulomb shift from non-nearest neighbors and the tip potential tend to decrease ε_1.

Turning our attention to 3DMs, the above results imply that we should expect, on average, $\varepsilon_1^{3DM} \approx -3^2 = -9\text{Ry}^*$. This is close to the observed peak near -7Ry^*, indicated by the left-most black arrow in Fig. 4(c). With regard to the magnitude of the 3DM first-electron peak, we expect it to scale approximately with the number of molecules. Fig. 4(c) shows the calculated magnitude of the first 2DM peak to be $7.5e/\text{Ry}^*$; hence we expect the first 3DM peak to be $\sim(12/26)7.5e/\text{Ry}^* = 3.5e/\text{Ry}^*$. This is approximately consistent with the observed magnitude of the peak near -7Ry^*. Hence we believe that this peak is likely the first 3DM resonance. No other 3DM peaks are as prominent in the measured data, likely due to the overlap between the 3DM and 2DM spectra. We believe some of the measured structure between $-6\text{Ry}^*$and 0Ry^*, such as the small peak near -5Ry^* (right-most black arrow), may arise from 3DMs. Small peaks also occur at positive energy, indicated by the light-gray arrows in Fig. 4(c). In this case, we speculate that the peaks arise from the interplay between the tip potential and donor-molecule resonant states (i.e., virtual bound states).

In summary, we have measured the electron addition spectrum of silicon donors in a gallium-arsenide heterostructure using a scanning probe technique. To analyze the data we have developed a theoretical model based on the idea that nearest-neighbor pairs effectively form TDMs. The model includes the influence of the tip and the broadening effect of non-nearest neighbor donors, predicting that three resonances will be observed due to four bound states per molecule. Comparing the measurement to the model, we find good qualitative and quantitative agreement in the shape and position of the most prominent addition spectrum peaks—suggesting that the 2DM model indeed captures the relevant physics. To the best of our knowledge this study represents the first measurement of the electron addition spectrum of donor molecules in a semiconductor system.

Acknowledgements

We gratefully acknowledge L.N. Pfeiffer and K. West, who provided the heterostructure sample used in Ref. [11], and R.C. Ashoori, N. Birge, M.I. Dykman, B. Golding, S.D. Mahanti, I.J. Maasilta, S. Rogge, and G.A. Steele, for helpful advice and comments. The work was supported by the Michigan State Institute for Quantum Sciences and the National Science Foundation, Grant nos. DMR-0305461 and DMR-0605801.

References

[1] B.E. Kane, Nature 393 (1998) 133.
[2] R. Vrijen, et al., Phys. Rev. A 62 (2000) 012306.
[3] L.C.L. Hollenberg, et al., Phys. Rev. B 69 (2004) 113301.
[4] F.J. Ruess, et al., Small 3 (2007) 563.
[5] S.E.S. Andresen, et al., Nano Lett. 7 (2007) 2000.
[6] W. Kohn, J.M. Luttinger, Phys. Rev. 98 (1955) 915.
[7] E.H. Lieb, Phys. Rev. A 29 (1984) 3018.
[8] M.R. Deshpande, J.W. Sleight, M.A. Reed, R.G. Wheeler, R.J. Matyi, Phys. Rev. Lett. 76 (1996) 1328.
[9] H. Sellier, et al., Phys. Rev. Lett. 97 (2006) 206805.
[10] A.K. Geim, et al., Phys. Rev. B 50 (1994) 8074.
[11] I. Kuljanishvili, et al., Nat. Phys. 4 (2008) 227.
[12] R.C. Ashoori, Nature 379 (1996) 413.
[13] R.C. Ashoori, et al., Phys. Rev. Lett. 68 (1992) 3088.
[14] S.H. Tessmer, P.I. Glicofridis, R.C. Ashoori, L.S. Levitov, M.R. Melloch, Nature 392 (1998) 51.
[15] S. Urazhdin, I.J. Maasilta, S. Chakraborty, I. Moraru, S.H. Tessmer, Rev. Sci. Instrum. 71 (2000) 4170.
[16] S.H. Tessmer, I. Kuljanishvili, Preprint, arXiv:0806.1899.
[17] T.A. Kaplan, J. Stat. Phys. 122 (2006) 1237.
[18] J. Hampton, J.P. Eisenstein, L.N. Pfeiffer, K.W. West, Solid State Commun. 94 (1995) 559.
[19] D.R. Lide, CRC Handbook of Chemistry and Physics, 86th ed., Taylor & Francis, Boca Raton, 2006.
[20] M.A. Eriksson, et al., Appl. Phys. Lett. 69 (1996) 671.
[21] I. Kuljanishvili, S. Chakraborty, I.J. Maasilta, S.H. Tessmer, Ultramicroscopy 102 (2004) 7.
[22] J.H. Davies, The Physics of Low-dimensional Semiconductors: an Introduction, Cambridge University Press, Cambridge, 1998.
[23] T. Schmidt, St.G. Muller, K.H. Gulden, C. Metzner, G.H. Dohler, Phys. Rev. B 54 (1996) 13980.
[24] J.C. Slater, Electronic Structure of Molecules, in: Quantum Theory of Molecules and Solids, vol. 1, McGraw-Hill, New York, 1963.
[25] T.H. Dunning, J. Chem. Phys. 90 (1989) 1007.
[26] M. Levinstein, S. Rumyantsev, M. Shur, Handbook Series on Semiconductor Parameters, vol. 2, World Scientific, London, 1999.
[27] S. Brandt, G. Gowan, Data Analysis: Statistical and Computational Methods for Scientists and Engineers, Springer, New York, 1999.